JOURNAL OF COMPUTATIONAL PHYSICS 54, 95–114 (1984)

Computation of Free Oscillations of the Earth

RAY BULAND

U.S. Geological Survey, Denver Federal Center, Denver, Colorado 80225

AND

FREEMAN GILBERT

University of California at San Diego,
Scripps Institution of Oceanography, La Jolla, California 92093

Received June 15, 1981

Although free oscillations of the Earth may be computed by many different methods, numerous practical considerations have led us to use a Rayleigh–Ritz formulation with piecewise cubic Hermite spline basis functions. By treating the resulting banded matrix equation as a generalized algebraic eigenvalue problem, we are able to achieve great accuracy and generality and a high degree of automation at a reasonable cost.

INTRODUCTION

Most of what is currently known about the detailed mechanical structure of the interior of the Earth has been learned from the study of elastic wave propagation. For frequencies of seismic interest (~0.3 mHz to 100 Hz) the source is generally either an earthquake or an explosion; the receivers are accelerometers, polarized either vertically or in one horizontal direction, placed at the Earth's surface.

In this paper we will be concerned with numerical modeling of very low frequency (~0.3–25 mHz) seismic energy. In this frequency band it is observationally and computationally convenient to consider a standing rather than a traveling wave formalism. That is, we will represent the displacement field in the interior of the Earth as a sum over the elastic–gravitational free oscillations (normal modes) of the Earth (for a review of this topic, see Buland [6]).

The computational effort involved in free oscillation modeling is completely dominated by the calculation of the normal mode eigenfunctions and eigenfrequencies themselves. In the following we will devote our attention exclusively to a Rayleigh–Ritz algorithm we have developed for solving this problem. Some of this work has been briefly described by Buland and Gilbert [4].

0021-9991/84 $3.00

581/54/1-7

MATHEMATICAL FORMULATION

Consider an Earth model which is spherically symmetric, self-gravitating, transversely isotropic, and slightly anelastic. If one computes all j elastic–gravitational free oscillations of this model having eigenfrequencies less than some cutoff angular frequency ω_c, then one may write (frequency) band limited, infinitesimal displacements in the interior of the model as

$$\mathbf{s}(r, \vartheta, \phi, t) = \sum_{k=1}^{j} e_k \mathbf{S}_k(r, \vartheta, \varphi)\, e^{(i\omega_k - \alpha_k)t}, \tag{1}$$

where $\mathbf{s}$ is displacement; r, ϑ, and φ are radius, co-latitude, and longitude respectively (i.e., the usual spherical coordinates), and t is time. e_k is the excitation, $\mathbf{S}_k$ the eigenfunction displacement, ω_k the angular eigenfrequency, and α_k the damping parameter of the kth free oscillation. Note that Eq. (1) is incomplete in fluid portions of the model as we have neglected the gravitational–elastic normal modes describing fluid flow. As all sources and receivers of seismological interest are located in solid regions of the Earth's interior, this need not concern us here.

From Rayleigh's principle, the normal modes we seek are extremal solutions of the energy balance equation

$$\omega^2 \int_0^a A(r)\, r^2\, dr - \int_0^a B(r)\, r^2\, dr = 0, \tag{2}$$

where $\omega^2 A$ is kinetic energy density, B is potential energy density, and a is the radius of the Earth model. Following Backus [1], we decompose the eigenfunction displacement into vector spherical harmonics

$${}_n\mathbf{S}_l^m(r, \vartheta, \varphi) = \hat{r}\, {}_nU_l(r)\, Y_l^m(\vartheta, \varphi) + {}_nV_l(r)\, \nabla_1 Y_l^m(\vartheta, \varphi) - {}_nW_l(r)\, \hat{r} \times \nabla_1 Y_l^m(\vartheta, \varphi), \tag{3}$$

where the mode index k has been replaced by the three indices n (radial order), l (angular order), and m (azimuthal order). U, V, and W are amplitude scalars for displacement in three locally orthogonal directions. The Y_l^m's are fully normalized surface harmonics. ∇_1 is the tangential gradient operator

$$\nabla_1 = \hat{\vartheta}\, \partial_\vartheta + \hat{\varphi} \csc \vartheta\, \partial_\varphi, \tag{4}$$

where ∂_x means the partial derivative with respect to x and $\hat{r}$, $\hat{\vartheta}$, and $\hat{\varphi}$ are unit vectors in the r, ϑ, and φ directions, respectively. Because the Earth model is self-gravitating it will be necessary to consider the perturbation to the gravitational potential due to displacement ${}_n\mathbf{S}_l^m$

$${}_nP_l^m(r, \vartheta, \varphi) = \hat{r}\, {}_nP_l(r)\, Y_l^m(\vartheta, \varphi). \tag{5}$$

The potential perturbation will have the same time dependence as the corresponding displacement.

Due to the spherical symmetry of the model, the problem thus reduces to one of determining scalers U, V, W, and P which are functions of radius alone and constants ω and α. Following Pekeris and Jarosch [14], but using the notation of Backus and Gilbert [2] and Backus [1], Eq. (2) may be rewritten as

$$\begin{aligned}
&\tfrac{1}{2}\omega^2 \int_0^a \rho(U^2 + V^2 + W^2)\, r^2\, dr - \int_0^a \{[(2\lambda' + 2\mu' - 2\rho g r + 2\rho^2 r^2) U^2 \\
&\quad + 2\lambda r U\dot{U} + \tfrac{1}{2}\beta r^2 \dot{U}^2 - \rho r^2 U\dot{P} + \tfrac{1}{2}(\mu - 2\mu')\, V^2 - \mu r V\dot{V} + \tfrac{1}{2}\mu r^2 \dot{V}^2 + \tfrac{1}{2}(\mu - 2\mu')\, W^2 \\
&\quad - \mu r W\dot{W} + \tfrac{1}{2}\mu r^2 \dot{W}^2 + \tfrac{1}{8}P^2 + \tfrac{1}{4} r P\dot{P} + \tfrac{1}{8} r^2 \dot{P}^2] \\
&\quad + L[(\rho g r - 2\lambda' - 2\mu' - \mu)\, UV + \mu r U\dot{V} - \lambda r \dot{U} V - \rho r V\dot{P}] \\
&\quad + L^2[\tfrac{1}{2}\mu U^2 + \tfrac{1}{2}(\lambda' + 2\mu')\, V^2 + \tfrac{1}{2}\mu' W^2 + \tfrac{1}{8}P^2] + l[\tfrac{1}{8}P^2 + \tfrac{1}{4} r P\dot{P}]\}\, dr = 0, \qquad (6)
\end{aligned}$$

where $\rho(r)$ is density; $\lambda(r), \lambda'(r), \mu(r), \mu'(r)$, and $\beta(r)$ are transversely isotropic Lamé parameters; $g(r)$ is the acceleration due to gravity; $L^2 = l(l+1)$; and $\dot{x}$ means the derivative of x with respect to radius. The normal modes we seek are extremal solutions to Eq. (6) subject to the boundary conditions that radial displacement, U, is continuous everywhere but the surface and potential perturbation, P, is continuous everywhere while tangential displacements V and W are continuous everywhere except at solid–fluid interfaces. Also tractions R, S, and T and potential "traction" Q must be continuous everywhere, where

$$\begin{aligned}
{}_nR_l(r) &= \beta\dot{U} + \frac{\lambda}{r}(2U - LV), \\
{}_nS_l(r) &= \mu\dot{V} + \frac{\mu}{r}(LU - V), \\
{}_nT_l(r) &= \mu\dot{W} - \frac{\mu}{r} W, \\
{}_nQ_l(r) &= \dot{P} + \frac{l+1}{r} P + 4\rho U.
\end{aligned} \qquad (7)$$

Note that Eqs. (6) and (7) have been non-dimensionalized such that π times the universal gravitational constant, G, is unity. The anelasticity of the Earth model will be incorporated approximately by assuming that the Lamé parameters are complex. Because the anelasticity is small, it will be a good approximation to treat only the real part of Eqs. (6) and (7) directly. The imaginary part can be adequately treated after-the-fact by means of first-order perturbation theory (e.g., Dziewonski and Anderson [8]). Considering anelasticity, then, only complicates Eqs. (6) and (7) to

the extent that the Lamé parameters will be slightly frequency dependent (e.g., Jeffreys [11]). To first order, the frequency dependence may be written

$$\gamma(r, \omega) = \gamma_0(r) + \ln(\omega)\, \delta\gamma(r), \tag{8}$$

where γ is any of $\lambda, \lambda', \mu, \mu'$, or β (Kanamori and Anderson [12]).

Because W does not occur in cross terms with U, V, or P in Eq. (6), further simplification is possible. As with most elastic problems there will be solutions where only W is non-zero and solutions where only W is identically zero. The first type of solution is termed a toroidal mode and is denoted ${}_nT_l^m$. The second type of solution is termed a spheroidal mode and is denoted ${}_nS_l^m$. Fluid regions will not support toroidal motion. However, spheroidal motion will be present throughout the interior of the Earth model.

For each mode type and each angular order $l = 0, 1, 2,...$, Eqs. (6) and (7) have infinitely many solutions. The lowest frequency of these is dubbed the fundamental (or gravest) mode of the series and assigned radial order zero. The higher frequency modes (overtones) are assigned successively higher, integral radial order numbers in order of increasing frequency. Because Eqs. (6) and (7) are independent of azimuthal order, each solution will be $2l + 1$-fold degenerate (i.e., $m = -l, -l + 1,..., +l$ will be degenerate in frequency).

Physical Properties

In order to properly model the elastic response of the Earth, it is necessary to consider constraints imposed by the physical behavior of the system. In this spirit, we will briefly review the types of normal modes we expect to find and how they interact with one another.

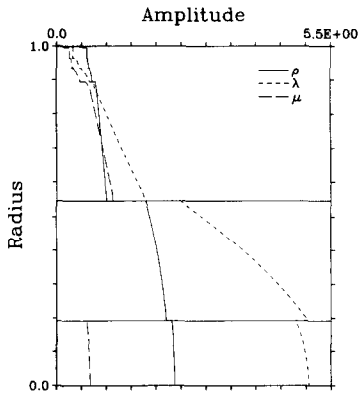

FIG. 1. Non-dimensional components λ, μ, and ρ of Earth model PREM [8] at a reference frequency of 1 Hz are plotted as a function of non-dimensional radius. The small anisotropy of this model has been averaged away for purposes of illustration.

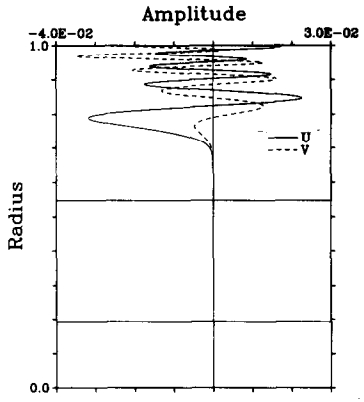

FIG. 2. Eigenfunction displacement for the mantle spheroidal mode ${}_9S_{100}$.

Figure 1 shows a typical, spherically averaged Earth model. In this diagram, the components of the model (density and the Lamé parameters) are plotted as a function of radius. Note that non-dimensional amplitude is drawn horizontally and normalized radius vertically. The surface of the model is at the top of the diagram, the center at the bottom. For purposes of illustration, the model is shown at a reference frequency of 1 Hz and the small transverse isotropy has been averaged away ($\lambda' = \lambda, \mu' = u, \beta = \lambda + 2\mu$).

The most important feature of Earth models is that all model parameters generally increase with depth. This also turns out to be true of the related parameters compressional and shear velocity. As a result, the most interesting and useful subset of free oscillations is oscillatory from the Earth's surface down to a depth related to the velocity of the medium and the phase velocity of the normal mode. Below this point the mode will be evenescent, decaying toward the Earth's center. Figures 2–4

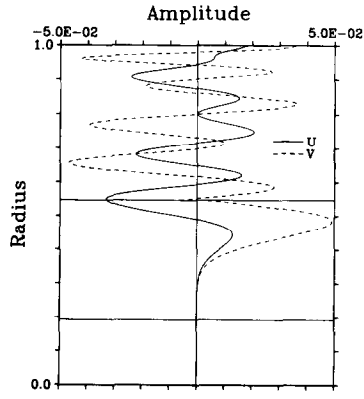

FIG. 3. Eigenfunction displacement for the spheroidal mode ${}_{14}S_{20}$. This mode penetrates into the outer core.

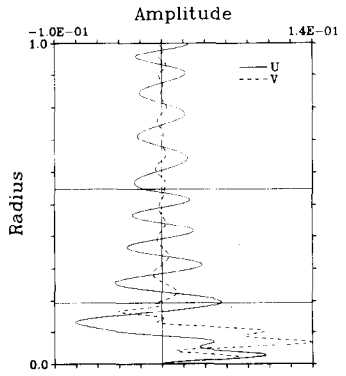

FIG. 4. Eigenfunction displacement for the spheroidal mode ${}_{39}S_3$. This mode penetrates into the inner core.

show a suite of such solutions. Each figure is laid out as in Fig. 1, but shows the radial scalars U and V for one spheroidal mode. All modes shown are computed using model 1066A of Gilbert and Dziewonski [10]. Amplitude is normalized so that kinetic energy equals $\frac{1}{2}\omega^2$. Phase velocity increases in successive figures and so does the depth of penetration into the model.

Unfortunately, this is not the only type of solution which must be considered. The two solid horizontal lines in the interior of Fig. 1 mark boundaries between physically distinct regions of the Earth's interior. The upper region is the solid mantle, the center region the fluid outer core, and the lower region the solid inner core. The presence of fluid–solid boundaries in its interior greatly complicates the Earth's elastic response. As a result, we must also consider solutions which are trapped in one region or on one of the boundaries. Figures 5 and 6 show modes trapped in the mantle and inner core (called core modes), respectively. Figures 7 and 8 show modes (called Stoneley modes) trapped on the core–mantle and inner core–outer core interfaces respectively.

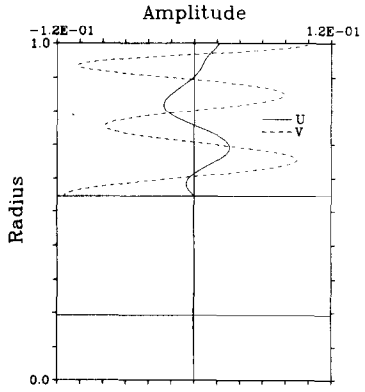

FIG. 5. Eigenfunction displacement for the spheroidal mode ${}_{14}S_3$. This mode is trapped in the mantle.

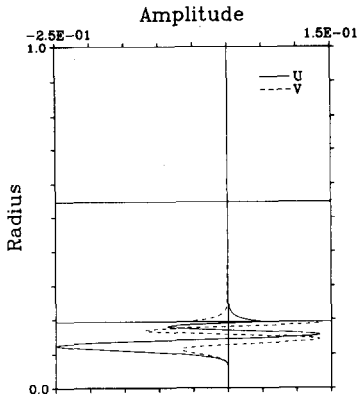

FIG. 6. Eigenfunction displacement for the spheroidal core mode ${}_{29}S_{20}$.

As one might expect, there are also solutions trapped in the fluid outer core. These are the fluid flow modes alluded to above, also known as gravitational–elastic modes or undertones. The behavior of these modes is sufficiently different from the elastic–gravitational modes of interest here that they are generally considered separately (e.g., Smith [17]). Therefore, we will not consider them further (although we will find that they cannot be entirely forgotten).

There is one additional complication which must be mentioned. As for any elastic solid, the Earth's mantle and inner core support two kinds of wave motion: compressional or longitudinal motion and shear or transverse motion. The fluid outer core and ocean support only compressional motion. Toroidal modes represent pure shear motion. Therefore, the fluid outer core will not support toroidal motion and toroidal mantle and core modes are entirely decoupled. As a result, toroidal core modes are generally neglected, a practice we will follow here. There are, then, toroidal analogs of Figs. 2, 5, and 6 but not of Figs. 3, 4, 7 and 8.

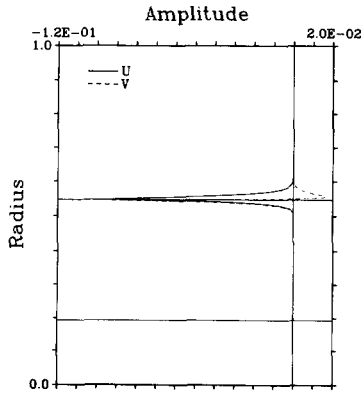

FIG. 7. Eigenfunction displacement for the core–mantle spheroidal Stoneley mode ${}_{8}S_{100}$.

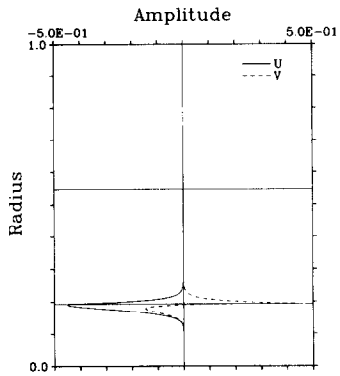

FIG. 8. Eigenfunction displacement for the inner core–outer core spheroidal Stoneley mode ${}_9S_{20}$.

The simplicity of toroidal modes may be seen by examining a dispersion diagram. Figure 9 shows a plot of the eigenfrequencies of mantle toroidal modes as a function of angular order. The dispersion curves are obtained by connecting the eigenfrequencies of modes with constant radial order. Fig. 9 may be considered to be a frequency–wavenumber diagram because angular order is asymptotically proportional to horizontal wavenumber as frequency becomes large. The slope of the dispersion curves is proportional to group velocity and straight lines passing through the origin are lines of constant phase velocity. Dashed line A is the phase velocity needed to penetrate to the base of the mantle. Modes to the left of this line are oscillatory everywhere in the mantle. Modes to the right of this line are evenescent below some depth.

Spheroidal dispersion might be expected to be considerably more complicated as spheroidal modes represent coupled compressional and shear motion. Figure 10 shows that this is indeed the case. Again we divide the diagram into regions. However, because of the coupling, the physical interpretation of these dividing lines is no longer simple. It is convienent to use the phase velocities of the Stoneley branches

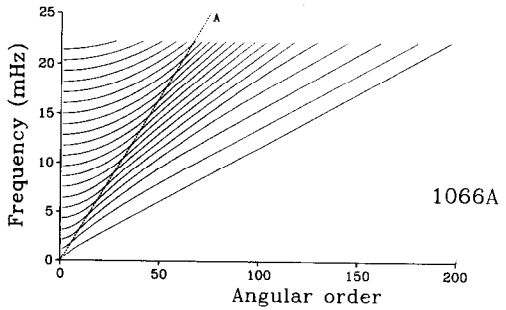

FIG. 9. Mantle toroidal mode dispersion diagram. Angular order is asymptotically proportional to horizontal wavenumber as $\omega \to \infty$. Dashed line A marks the phase velocity needed for a mode to penetrate to the base of the mantle.

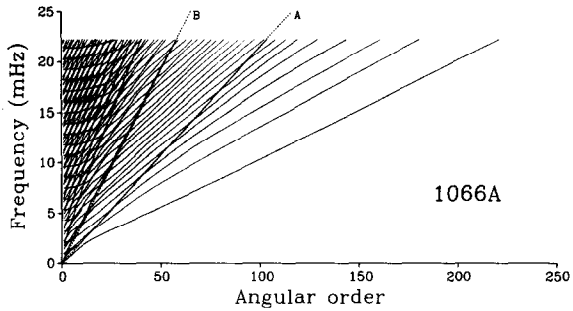

FIG. 10. Spheroidal mode dispersion diagram. Dashed line A marks the phase velocity of core–mantle Stoneley modes. Dashed line B marks the phase velocity of inner core–outer core Stoneley modes.

for this division. Dashed line A marks the phase velocity of the core–mantle Stoneley modes (see Fig. 7). Dashed line B marks the phase velocity of the inner core–outer core Stoneley modes (see Fig. 8). To the right of A, compressional and shear motion are strongly coupled resulting in remarkable similarity to the corresponding region of Fig. 9. To the left of A the lines of constant radial order have sharp bends forming a stair step pattern. Although they never cross, segments of these lines conspire to form trends which are smoothly varying across the diagram. To the left of B one can pick out many subparallel instances of three distinct trends, resulting from much weaker coupling between compressional and shear motion in this region. The shallowest trend represents the dispersion of mantle shear waves, the intermediate trend that of whole Earth compressional waves, and the steepest that of inner core shear waves.

Although the Earth is known to possess structural details at all scale lengths, structure other than that discussed above modifies dispersion rather than contributing new kinds of solutions at normal mode frequencies. Structure with scale lengths smaller than about 50 km in radius and 1000 km tangentially is generally quite insignificant at the frequencies of interest here.

ALGORITHMIC CONSTRAINTS

As stated above, toroidal core modes and fluid undertones will be neglected. However, because of the coupling among various types of spheroidal modes, we have resolved to compute all of them, even though many have small expression at the Earth's surface. Second, because of the large number of modes of interest (~6000 with eigenfrequency less than 25 mHz), a high degree of automation is required. Third, because many high phase velocity spheroidal modes with the same angular order form doublets or triplets with nearly the same eigenfrequency (see Fig. 10), we require a method which properly handles near degeneracy in eigenfrequency. Fourth, a high degree of precision in the eigenfrequency is required as observations are

achieving accuracies of a few parts per million in some cases (e.g., Buland *et al.* [5]). Finally, the method must be reasonably efficient.

Most of these criteria ultimately caused us to abandon many years experience with a shooting method in favor of a Rayleigh–Ritz approach. Shooting methods generally lack the required degree of automation because both the direction of stable integration and the appropriate place for matching the boundary conditions are mode dependent (e.g., compare Figs. 2 and 7). Second, it is quite possible for a shooting method to interpret a triplet as a single solution and to miss a doublet altogether. Finally, shooting methods can become very inefficient if one requires high precision at high angular order. This is because normal mode amplitude in an evenescent region decays as r^l (l can reach 250 for modes with eigenfrequency less than 25 mHz), making the system very "stiff."

Instead we use a Rayleigh–Ritz formulation and solve the resulting matrix equation as an algebraic eigenvalue problem. This provides full automation and completely correct handling of nearly degenerate eigenfrequencies. Furthermore, the stiffness problem is alleviated by the fact that the observable eigenfrequency is found to twice the significance of the non-observable eigenfunction.

It is worth noting that Woodhouse [20] has removed two of our objections to shooting methods. He achieves full automation by reformulating the problem in terms of minors (e.g., Gilbert and Backus [9]). Further, he was able to define an analog of the Sturm count computed directly from a trial eigenfunction. This allows proper handling of nearly degenerate eigenfrequencies.

Numerical Formulation

Following Wiggins [18], we have chosen to use the basis functions for piecewise cubic Hermite interpolation (H-splines) as basis functions for our Rayleigh–Ritz problem (Birkhoff, *et al.* [3]). These are the lowest-order polynomial basis functions which allow all boundary conditions to be matched exactly, as required by the classical Rayleigh–Ritz method. Furthermore, each H-spline is of limited spatial extent (a finite element). This allows sufficient generality to encompass all possible types of solution and leads to a computationally efficient, banded matrix problem.

In order to specify the problem in detail it is useful to consider three radial discretations of the Earth model. First, consider interface grid, η. Each element of η is a radius at which one or more components of the model is discontinuous.

$$\eta: \qquad 0 = z_1 < z_2 < \cdots < z_K = a. \tag{9}$$

Second, consider model grid, v

$$v: \qquad 0 = y_1 < y_2 < \cdots < y_M = a. \tag{10}$$

It has proven sufficiently general to think of Earth models as being specified only at the M points of v. In keeping with the H-spline basis functions, we interpolate each

element of the model over grid ν with a piecewise cubic polynomial (B-splines) which fits the model parameter exactly at points of ν and has continuous first and second derivatives everywhere (Carasso and Laurent [7]). In order that the model be properly interpolated it is necessary that grid η be a subset of grid ν and that the B-spline interpolation be broken at each interface.

Finally, consider H-spline grid π

$$\pi: \qquad 0 = x_1 < x_2 < \cdots < x_N = a. \tag{11}$$

For each radial function to be represented, say $F(r)$, we need $2N$ basis functions, two centered at each point of grid π. That is,

$$F(r) \approx \sum_{i=1}^{N} \{F_i \chi_i(r) + \dot{F}_1 \psi_i(r)\}, \tag{12}$$

where F_i and $\dot{F}_i$ are constants and χ_i, ψ_i, $i = 1, 2, \ldots, N$ are the $2N$ basis functions.

Define normalized H-splines

$$\chi_0(x) = \begin{cases} 2x^3 - 3x^2 + 1, & 0 \leqslant x \leqslant 1 \\ -2x^3 - 3x^2 + 1, & -1 \leqslant x < 0 \\ 0, & \text{otherwise,} \end{cases}$$

$$\psi_0(x) = \begin{cases} x^3 - 2x^2 + x, & 0 \leqslant x \leqslant 1 \\ x^3 + 2x^2 + x, & -1 \leqslant x < 0 \\ 0, & \text{otherwise.} \end{cases} \tag{13}$$

χ_0 and ψ_0 are shown in Fig. 11 and their properties at grid points are summarized in Table I. The basis functions may now be written as

$$\chi_i(x) = \begin{cases} \delta_i \chi_0\left(\dfrac{x - x_i}{x_{i+1} - x_i}\right), & x \geqslant x_i \\ \chi_0\left(\dfrac{x - x_i}{x_i - x_{i-1}}\right), & x < x_i, \end{cases}$$

$$\psi_i(x) = \begin{cases} \delta_i (x_{i+1} - x_i)\, \psi_0\left(\dfrac{x - x_i}{x_{i+1} - x_i}\right), & x \geqslant x_i \\ (x_i - x_{i-1})\, \psi_0\left(\dfrac{x - x_i}{x_i - x_{i-1}}\right), & x < x_i, \end{cases} \tag{14}$$

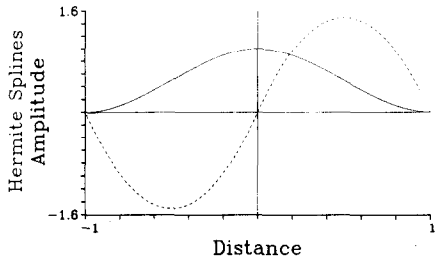

FIG. 11. The solid line is normalized H-spline χ_0 and the dashed line is ψ_0. The grid points are at $x = -1, 0, +1$.

where δ_i and $\dot{\delta}_i$ are additional constants which will be preselected to match the boundary conditions. Notice, if we select constants F_i, $\dot{F}_i$, δ_i, and $\dot{\delta}_i$ such that

$$\begin{aligned} F_i &= F(x_i^-), \qquad \delta_i F_i = F(x_i^+), \\ \dot{F}_i &= \dot{F}(x_i^-), \qquad \dot{\delta}_i \dot{F}_i = \dot{F}(x_i^+), \end{aligned} \tag{15}$$

then Eq. (12) is just the H-spline interpolation of $F(r)$. Since boundary conditions can only be matched at points of grid π, it is necessary that grid η be a subset of grid π. At interface points, δ_i and $\dot{\delta}_i$ will be chosen to match the boundary conditions relevant to the scalar being represented. Otherwise, $\delta_i = \dot{\delta}_i = 1$ will ensure the continuity of the scalar and its first derivative.

It is common practice in this sort of problem to make the ν and π grids coincide. There is, in fact, no necessity and little practical advantage in doing so. Therefore, we have chosen the conceptually more satisfying course of letting them be distinct. The ν grid must be chosen so that the B-spline interpolation of the model is sufficiently accurate. That is, the grid spacing must be dense where the model parameters vary rapidly and may be sparse where the model parameters are smooth. In practice, we generally use a grid specified by the author of the model, if available, as we then make maximum use of all available information. In any case, it is generally worthwhile to err on the side of caution as the efficiency of B-spline interpolation is only a weak function of grid size M.

Selection of the π grid is quite another problem. If N is too small, there will not be

TABLE I

Normalized H-Spline Values at Selected Grid Points

x	$\chi_0(x)$	$\partial_x\chi_0(x)$	$\psi_0(x)$	$\partial_x\psi_0(x)$
−1	0	0	0	0
0	1	0	0	1
+1	0	0	0	0

enough basis functions to adequately represent the desired eigenfunctions causing a loss of precision. If N is too large, the resulting matrix problem will be larger and more costly to solve than necessary. It is possible to optimize π by making the local grid spacing $h_i = x_{i+1} - x_i$ proportional to the minimum radial wavelength of interest. That is, where an eigenfunction is oscillatory it will always have at least I grid points ($2I$ degrees of freedom) per wavelength if

$$h_i = \left(\frac{1}{I \cdot f_{\max}} \int_{x_i}^{x_{i+1}} v_{\min}(r)\, dr \right)^{1/2}, \tag{16}$$

where $f_{\max}$ is the maximum frequency of interest and $v_{\min}$ is the minimum velocity of the medium (shear velocity in solids, compressional velocity in fluids). Although Eq. (16) is not necessarily justified in evenescent regions of an eigenfunction, it turns out to work well in practice as long as I is sufficiently large.

Formulation of the matrix problem is now straightforward. After selecting I and $f_{\max}$, construct grid π using Eq. (16). Then expand scalers U, V, W, and P in the basis functions (Eq. (14)) as in Eq. (12). Unfortunately the constants δ_i and $\dot{\delta}_i$ for each scalar may depend on angular order and on eigenfrequency for interface grid points (see Eq. (7)). If they are specified at this stage, it will be necessary to perform the integrals in Eq. (6) for each angular order and trial eigenfrequency. The problem is avoided by breaking basis functions which span an interface grid point, say x_j, into two portions each: $\chi_j(r)$ becomes $\chi_j(r \leqslant x_j)$ and $\chi_j(r \geqslant x_j)$, $\psi_j(r)$ becomes $\psi_j(r \leqslant x_j)$ and $\psi_j(r \geqslant x_j)$. Treating each fractional basis function independently defers the specification of the δ_j's and $\dot{\delta}_j$'s until a more convenient time.

The same problem clearly affects the integrand of Eq. (6) itself. The l dependence is shown explicitly. The frequency dependence of Eq. (6) will be the same as that of the Lamé parameters (shown in Eq. (8)).

Therefore, Eq. (2) may be rewritten as

$$\omega^2 \int_0^a A(r)\, r^2\, dr - \int_0^a \{B_0(r) + LB_1(r) + L^2 B_2(r) + lB_3(r) + \ln(\omega)[\delta B_0(r) + L\delta B_1(r) + L^2 \delta B_2(r)]\}\, r^2\, dr = 0, \tag{17}$$

where A, the B_j's, and the δB_j's are all independent of l and ω. Notice that A and B_3 are frequency independent as they contain only inertial terms.

Because a basis function associated with grid point x_j interacts only with itself and its nearest neighbors (basis functions associated with grid points x_{j-1}, x_j, and x_{j+1}), it is convenient to perform the integrals in Eq. (17) over the subintervals $[x_j, x_{j+1}]$, $j = 1, 2, \ldots, N-1$. On each subinterval the integral is computed by a 6-point Gauss–Legendre quadrature. This method is very fast, stable, and accurate. In fact, it is exact for polynomials up to order 11. It can never be exact in our case, though, even if the v and π grids were made to coincide, because the gravitational acceleration, g, will be a rational polynomial if density is a simple polynomial. It is, however, accurate enough for our purposes.

Performing the integrals in Eq. (17) yields the corresponding matrix equation

$$(\omega^2\mathbf{A} - \{\mathbf{B}_0 + L\mathbf{B}_1 + L^2\mathbf{B}_2 + l\mathbf{B}_3 + \ln(\omega)[\delta\mathbf{B}_0 + L\delta\mathbf{B}_1 + L^2\delta\mathbf{B}_2]\}) \cdot \mathbf{b} = 0 \quad (18)$$

where the $\mathbf{A}$, the $\mathbf{B}_j$ and the $\delta\mathbf{B}_j$ matrices are independent of l and ω and so need be computed only once per model. The eigenvalue ω^2 is clearly just eigenfrequency squared. The eigenvector $\mathbf{b}$ will contain all of the coefficients needed to specify the linear combinations of basis functions representing each scalar component of the computed eigenfunction.

Choosing one angular order and, for the moment, neglecting the frequency dependence of the model, we may rewrite Eq. (18) as

$$[\omega^2\mathbf{A} - \mathbf{B}] \cdot \mathbf{b} = 0. \quad (19)$$

Equation (19) is not quite in final form because the boundary conditions have not yet been matched. They can be matched directly in matrix $\mathbf{A}$ by forming the appropriate linear combination of rows and columns, eliminating rows and columns which are no longer needed, to form transformed matrix $\tilde{\mathbf{A}}$. Likewise $\mathbf{B}$ is transformed into $\tilde{\mathbf{B}}$ yielding

$$\mathbf{C}(\omega) \cdot \mathbf{b} = [\omega^2\tilde{\mathbf{A}} - \tilde{\mathbf{B}}] \cdot \mathbf{b} = 0. \quad (20)$$

Since $\tilde{\mathbf{A}}$ is not diagonal, this is a generalized eigenvalue problem. However, because of our choice of basis functions both matrices are sparse and, in fact, can be rearranged to be block diagonal. Each block will be of dimension $2J \times 4J$, where J is the number of scalars (coupled second-order ordinary differential equations) involved. As there are N blocks, the problem has dimension $2JN \times 2JN$.

Following Martin and Wilkinson [13], $\mathbf{C}(\omega)$ may be triangularized, in order NJ^3 operations, for each trial ω, preserving both its sparseness and its Sturm count (number of eigenvalues larger than the trial value). Following Peters and Wilkinson [15], the Sturm count and determinant of $\mathbf{C}$ may be used to locate an eigenvalue to machine precision by a combination of bisection and linear interpolation. The performance of this algorithm depends critically on the matrix decomposition. We can improve the performance of the decomposition by about 30% by reducing the bandwidth of $\mathbf{C}$ prior to triangularization using an algorithm due to Schwarz [16]. Given an eigenvalue, the corresponding eigenfunction is found by inverse iteration (Wilkinson [19]) using the final matrix decomposition needed in the bisection.

Because matrix $\mathbf{C}$ is constructed and decomposed for each trial eigenfrequency, there is no difficulty incorporating a small frequency dependence into the $\mathbf{B}$ matrix. Note that in the frequency-independent case it is necessary to match boundary conditions in matrix $\mathbf{B}$ only once per angular order. In the frequency-dependent case the boundary conditions must be matched once per trial eigenfrequency. The additional work required has a negligible impact on performance because matching the boundary conditions is insignificant compared with decomposing matrix $\mathbf{C}$.

It is interesting to note that the frequency-dependent problem (Eq. 18)) is a peculiar eigenvalue problem. Because of the frequency dependence, a different eigenvalue problem is, in effect, being examined at each trial eigenfrequency. This peculiarity leads to no complications in practice because the frequency dependence of **B** is very slight. However, it does have the result that our final eigenvectors will not be orthogonal.

Numerical Performance

Following a finite element rule-of-thumb (G. Frazier, personal communication, 1975), we require at least six points of grid π per radial wavelength ($I = 6$). Although we desire higher accuracy than is typical of finite element calculations, our choice turns out to be conservative. This is because finite element programs usually use piecewise linear basis functions providing $O(h^2)$ accuracy in eigenfrequency where

$$h = \| h_j \|. \tag{21}$$

H-splines, however, can be shown to provide $O(h^6)$ accuracy in the eigenfrequency and $O(h^3)$ in the eigenfunction (Birkhoff *et al.* [3]).

Numerical experiments indicate that the algorithm of Peters and Wilkinson [15] routinely finds eigenvalues to about one part in 10^{11} (for a machine truncation of about one part in 10^{14}). However, the numerical eigenfrequency will always be an upper bound to the actual eigenfrequency (e.g., Birkhoff *et al.* [3]). Therefore, absolute accuracy must be determined by other means. In order to assess the absolute accuracy of computed eigenfrequencies, we compared the results of the Rayleigh–Ritz algorithm with those of a shooting method due to Gilbert. The shooting program is capable of an absolute accuracy in the eigenfrequency of about one part in 10^7 (limited by the precision to which Runge–Kutta coefficients are specified). Even for eigenfrequencies in the vicinity of $f_{\max}$, the two methods were always found to agree to at least seven significant figures.

Experience in computing free oscillations of the Earth shows that the size of the π grid will be

$$N \approx 1.2I \cdot f_{\max} \tag{22}$$

for spheroidal modes and

$$N \approx 0.7I \cdot f_{\max} \tag{23}$$

for mantle toroidal modes, where $f_{\max}$ is in millihertz. If one wishes to compute all elastic–gravitational spheroidal and mantle toroidal modes with eigenfrequency less than $f_{\max}$, there are about $12 f_{\max}^2$ modes to determine. Of these roughly two-thirds will be spheroidal and one-third toroidal. The performance of our Rayleigh–Ritz algorithm is determined by the matrix decomposition needed to find the determinant

TABLE II

Computational Effort

Type of calculation	J	Relative effort, E
Mantle toroidal	1	0.07
Spheriodal (neglecting P)	2	1.9
Spheriodal (including P)	3	6.3

and Sturm count of $\mathbf{C}(\omega)$ at each trial ω. Roughly, a constant 12 matrix decompositions are required per computed normal mode. Combining the results of this section, we may determine the relative effort required to compute suites of normal modes under various assumptions. These results are shown in Table II. Relative effort, E, is normalized so that

$$T = E \cdot I \cdot f_{\max}^3 \tag{24}$$

will be approximate CPU time in seconds on a VAX 11/780 minicomputer.

Without any other economies, if we choose I to be 6 and $f_{\max}$ to be 25 mHz, our worst case calculation will require about 170 hours CPU on the VAX minicomputer. While this is a lot of computer time, it is by no means out of reach considering it need be done only once per model for a small number of models. Of course, other economies are possible. However, since the most correct calculation is practical, we do not consider them to be viable for eigenfrequencies less than 25 mHz unless they entail no loss of accuracy. As normal mode calculations are extended beyond 25 mHz these arguments are no longer valid. Not only does the cost of the calculations increase as $f_{\max}^3$, but the number of models of interest increases dramatically as lateral structural variations become important. Fortunately, precision is less critical in this regime since observations are less accurate than in the normal

improving the performance of our algorithm by at least an order of magnitude.

Numerical Difficulties

The most pervasive problem with our algorithm is the occurrence of what Wiggins [18] calls "extraneous" roots. That is, eigenfrequencies occur throughout the eigenspectrum of matrix $\mathbf{C}$ (but most commonly at the lower frequencies) which do not correspond to any known elastic–gravitational normal mode. These "extraneous" modes have eigenfunctions whose energy is concentrated almost exclusively in the fluid outer core, leading Wiggens [18] to conclude that they arose because the radial derivative of the tangential displacement scalar V is poorly constrained in fluid regions. However, it is easy to show that this is not the cause of the problem. We

have done so by constraining V with a zero curl (so called Adams–Williamson) condition in the outer core.

The problem is actually mathematical rather than numerical. As discussed above, there are an infinite number of undertones with nearly zero eigenfrequency corresponding to flow in the Earth's fluid regions. While Eq. (6) incorporates approximations which are not valid for the undertones, it still has solutions which correspond to them. We can demonstrate that the "extraneous" modes are these solutions by locating an identifiable suite of them. In order to minimize computation, we have done this by constructing an Earth model with a stable outer core (Brunt–Vaisäla period of 6 hr). In this way, we were able to easily locate the first 10 (least oscillatory) undertones of angular order three. The least oscillatory of these is shown in Fig. 12.

The "extraneous" modes appear throughout the eigenspectrum because of the upper bound property of the Rayleigh–Ritz eigenfrequencies. Even in our finite dimensional basis space, there are a very large number of undertones. They very quickly become so oscillatory that no linear combination of basis functions can adequately represent them. As a result, their eigenfrequency estimates can become so poor that they may appear anywhere in the eigenspectrum. Although we have identified the source of the "extraneous" modes, we have found no means of factoring them out of the problem. Rather we have had to be content with indentifying and discarding them after the fact. This turns out to be quite simple to do using the fraction of kinetic energy in fluid regions as a discriminant.

The problem that Wiggins [18] was concerned about can occur also, though not in our experience in the outer core. However, it does lead to ill-conditioning in the ocean layer which can become severe enough to cause the matrix decomposition algorithm of Martin and Wilkinson [13] to fail. We eliminate this problem by applying a zero curl constraint in the model ocean. Although this condition is strictly correct only if the ocean is neutrally stratified (zero Brunt–Vaisäla frequency), the ocean layer is

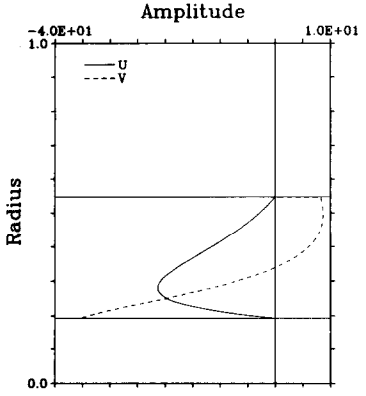

FIG. 12. Eigenfunction displacement for the least oscillatory spheroidal undertone of angular order three ($_{-1}S_3$).

sufficiently unimportant at normal mode frequencies that it makes no practical difference.

A related problem can occur in the Earth's outer core. Because the compressional velocity in the outer core is higher than the shear velocity anywhere in the Earth, our algorithm for constructing grid π can result in very sparse sampling of the outer core if the total number of grid points, N, is small. When the evenescent portion of a very low frequency mode penetrates the sparsely sampled outer core, the weak constraint on V allows large numerical ocillations in the eigenfunction. This problem does not occur for any mode if N is sufficiently large. For production work where $f_{\max}$ is of order 20 mHz this problem never arises. It can be avoided in experiments with low $f_{\max}$ by raising I in the outer core.

A final difficulty is mentioned more as a curiosity than a problem to be avoided. Comparing Figs. 7 and 12 it is clear that Stoneley modes and undertones may overlap spatially. As we have shown above, they also may have similar eigenfrequencies, at least numerically. Therefore, it is theoretically possible to have quasi-degenerate coupling between them. This has occurred once in our experience out of 7000 spheroidal modes calculated. The coupling results in two modes with nearly the same eigenfrequency, each having the character of both a Stoneley mode and an undertone. The cure for this problem is as simple as the problem is rare. Altering almost any aspect of the calculation should eliminate the coupling. Adding an extra grid point almost anywhere works quite nicely.

Economies

Several obvious economies readily present themselves. It is possible that the number of basis functions per radial wavelength, I, may be lowered with acceptable losses in accuracy (decreasing the size of the matrices). Likewise, it is possible to alter the tolerance to which eigenvalues are located as they are upper bounds of the true solution anyway (decreasing the number of matrix decompositions). We have chosen, instead, to pursue enhancements in performance which entail no loss in the accuracy of the result.

A time honored method of reducing the cost of computing spheroidal normal modes is to neglect the perturbation to the gravitational potential, P. The potential perturbation is really significant only at the very lowest frequencies. The economy gained can be substantial as shown by Table II. We have found two different methods of retaining the exact potential perturbation at little more than the cost of neglecting it.

The fastest method (and the one with which we have production experience) is useful only for frequency-independent Earth models. We begin by computing all spheroidal modes with eigenfrequency less than $f_{\max}$ for one angular order. Given displacement scalers U and V, there is an analytical expression for constructing the corresponding P (Pekeris and Jarosch [14]). The resulting eigenfunctions are now used as basis functions for a new Rayleigh–Ritz calculation. This time the matrices

are not sparse. However, they are always of dimension less than about $3f_{max}$. Surprisingly, all solutions of the new Rayleigh–Ritz problem are useful if f_{max} is sufficiently large. This is because the effect of P is quite small for eigenfrequencies larger than several millihertz. Although the gravest eigenfrequency may shift substantially, it still retains an accuracy of one part in 10^7 if f_{max} is large enough. This method fails for frequency-dependent models as it presumes that the desired eigenfunctions are orthogonal.

A more general method, applicable to frequency-dependent models, is suggested by the complete independence of the algorithms for determining eigenvalues and eigenvectors. As before, we begin by computing spheroidal modes neglecting P. Then, we reconstruct the H-spline Rayleigh–Ritz matrices including the potential perturbation terms. If the previously computed eigenfunction and eigenfrequency are sufficiently good, they may be refined to the complete solution by successive Rayleigh quotients and inverse iterations. In most cases, we expect that one matrix decomposition will suffice for the successful refinement. This method will probably fail for the very lowest frequency modes. In these cases the modes can be computed directly, including P. Even so, substantial savings should result overall from this technique.

A commonly used method of reducing the cost of finite element calculations in general is the lumped mass approximation. That is, the kinetic energy matrix is artificially diagonalized by assuming that mass is concentrated at points of the π grid. Elastic restoring forces and hence the potential energy matrix are left unchanged. The lumped mass approximation makes it possible to reduce our eigenvalue problem to standard form without enlarging the bandwidth. For a frequency-independent model, the calculation would require one matrix decomposition per angular order rather than 12 per normal mode.

The lumped mass approximation has a surprisingly small effect on dispersion (eigenfrequencies) because total mass is conserved and because the kinetic energy matrix is diagonally dominant anyway. In cases where a large number of modes is needed and extreme accuracy is not required, the approximate modes may be a satisfactory end product. If so, the effects of the approximation may be minimized by greatly expanding the π grid. Because the matrix need be decomposed only once per angular order, its size is no longer of primary importance. Second, the dispersion due to a frequency dependence in the model could be incorporated very satisfactorily in many cases by means of first-order perturbation theory.

In calculations where the lumped mass approximation is not accurate enough, it may be possible to parallel the scheme described above. That is, the approximate modes may be useful as starting solutions for a combination of Rayleigh quotients and inverse iterations converging to the most correct possible solution.

SUMMARY

We have used a Rayleigh–Ritz formulation with piecewise cubic Hermite spline basis functions to compute elastic–gravitational free oscillations of the Earth. Special

cases and nearly degenerate eigenfrequencies are property treated by posing the problem as a generalized algebraic eigenvalue calculation leading to a high degree of automation. The algorithm can be made reasonably efficient by utilizing the sparseness of the matrices. Although one must be cautious of stability problems in the fluid regions of an Earth model, no insurmountable problems arise. Significant economies are possible without loss in the completeness or accuracy of the solution by taking advantage of the independence of the eigenvalue and eigenvector computations.

ACKNOWLEDGMENTS

Development of our algorithm was aided by useful discussions with Jerry Frazier and Ralph Wiggins. The work was supported at various time by grants from NSF and AFOSR. The manuscript equations and text were computer typeset by Madeleine Zirbes.

REFERENCES

1. G. E. BACKUS, *Geophys. J. Roy. Astronom. Soc.*, **13** (1967), 71–101.
2. [illegible]
3. [illegible]
188–203.
4. R. P. BULAND AND F. GILBERT, *in* "Retrieving the Seismic Moment Tensor," Ph. D. thesis, University of California, San Diego, 1976.
5. R. BULAND, J. BERGER, AND F. GILBERT, *Nature*, **277** (1979), 358–362.
6. R. BULAND, *Ann. Rev. Earth Planet. Sci.* **9** (1981), 385–413.
7. C. CARASSO AND P. J. LAURENT, "Proc. IFIP Congress," North–Holland, Amsterdam, 1968.
8. A. M. DZIEWONSKI AND D. L. ANDERSON, *Phys. Earth Planet. Interiors* **25** (1981), 297–356.
9. F. GILBERT AND G. E. BACKUS, *Geophysics* **31** (1966), 326–332.
10. F. GILBERT AND A. M. DZIEWONSKI, *Phil. Trans. Roy. Soc. London A* **278** (1975), 187–269.
11. H. JEFFREYS, *Nature* **208** (1965), 675.
12. H. KANAMORI AND D. L. ANDERSON, *Rev. Geophys. Sp. Phys.* **15** (1977), 105–112.
13. R. S. MARTIN AND J. H. WILKINSON, *Numer. Math.* **9** (1967), 279–301.
14. C. L. PEKERIS AND H. JAROSCH, *in* "Contributions in Geophysics in Honor of Beno Gutenberg." Pergamon, Los Angeles, 1958.
15. G. PETERS AND J. H. WILKINSON, *Comput. J.* **12** (1968), 398–404.
16. H. R. SCHWARZ, *Numer. Math.* **12** (1968), 231–241.
17. M. L. SMITH, *Geophys. J. Roy. Astronom. Soc.* **37** (1974), 491–526.
18. R. A. WIGGINS, *Geophys. J. Roy. Astronom. Soc.* **47** (1976), 135–150.
19. J. H. WILKINSON, "The Algebraic Eigenvalue Problem," Clarendon, Oxford, 1965.
20. J. H. WOODHOUSE, *in* "Physics of the Earth's Interior," (A. M. Dziewonski and E. Boschi, Eds.), Elsevier, New York, 1980.